

# Coupling Navier-Stokes and Gross-Pitaevskii equations for the numerical simulation of two-fluid quantum flows

Marc Brachet<sup>1</sup>, Georges Sadaka<sup>2</sup>, Zhentong Zhang<sup>2</sup>,  
Victor Kalt<sup>2</sup> and Ionut Danaila<sup>2,\*</sup>

<sup>1</sup>ENS, Université PSL, CNRS,  
Sorbonne Université, Université de Paris,  
Laboratoire de Physique de l'École Normale Supérieure,  
F-75005 Paris, France.

<sup>2</sup>Univ Rouen Normandie, CNRS,  
Laboratoire de Mathématiques Raphaël Salem,  
UMR 6085, F-76000 Rouen, France

\* Corresponding author: [ionut.danaila@univ-rouen.fr](mailto:ionut.danaila@univ-rouen.fr)

November 14, 2022

## Abstract

Numerical methods for solving the Navier-Stokes equations for classical (or normal) viscous fluids are well established. This is also the case for the Gross-Pitaevskii equation, governing quantum inviscid flows (or superfluids) in the zero temperature limit. In quantum flows, like liquid helium II at intermediate temperatures between zero and 2.17 K, a normal fluid and a superfluid coexist with independent velocity fields. The most advanced existing models for such systems use the Navier-Stokes equations for the normal fluid and a simplified description of the superfluid, based on the dynamics of quantized vortex filaments,

with ad hoc reconnection rules. There was a single attempt (C. Coste, The European Physical Journal B - Condensed Matter and Complex Systems, 1998) to couple Navier-Stokes and Gross-Pitaevskii equations in a global model intended to describe the compressible two-fluid liquid helium II. We present in this contribution a new numerical model to couple a Navier-Stokes incompressible fluid with a Gross-Pitaevskii superfluid. Coupling terms in the global system of equations involve new definitions of the following concepts: the regularized superfluid vorticity and velocity fields, the friction force exerted by quantized vortices to the normal fluid, the covariant gradient operator in the Gross-Pitaevskii based on a slip velocity respecting the dynamics of vortex lines in the normal fluid. A numerical algorithm based on pseudo-spectral Fourier methods is presented for solving the coupled system of equations. Finally, we numerically test and validate the new numerical system against well-known benchmarks for the evolution in a normal fluid of different types or arrangements of quantized vortices (vortex crystal, vortex dipole and vortex rings). The new coupling model has the advantage to keep the full Gross-Pitaevskii model for the superfluid, and thus describe quantized vortex dynamics without any phenomenological approximation. This opens new possibilities to revisit and enrich existing numerical results for complex quantum fluids, such as quantum turbulent flows.

## 1 Introduction

Realistic numerical models for quantum flows, such as liquid helium below the critical (lambda) temperature  $T_\lambda = 2.17K$ , have to accommodate with the celebrated two-fluid model (Tisza, 1938; Landau, 1941) stating that two fluids with independent velocity fields coexist in the system: a *normal* viscous fluid and an inviscid *superfluid*. If each component is taken separately, governing equations and numerically models are universally accepted: the Navier-Stokes (NS) equations for the normal fluid (the only one present in helium if  $T > T_\lambda$ ) and the Gross-Pitaevskii (GP) equation for the superfluid (dominant for  $T < 0.3K$ ). For intermediate temperatures, both components are present, with different physics. In the superfluid, quantized vortices are nucleated with fixed (quantized) circulation and fixed core diameter (of the atomic size). Complex interactions between quantized vortices tangled in space can lead to Quantum Turbulence (QT). In the normal fluid, vortices or eddies can

develop covering characteristic scales from the Kolmogorov viscous scale up to the container size and eventually generate turbulence. Note that the GP equation is known to well describe low- $T$  co-flow QT (Nore et al., 1997a,b; Clark di Leoni et al., 2017; Kobayashi et al., 2021) and can be extended to describe helium equation of state and dispersion law at zero temperature (Berloff et al., 2014).

Existing numerical models for quantum two-fluid flows either focus on a single component (using NS or GP models) or simplify the physics of one component in the two-fluid setting. The Hall–Vinen–Bekharevich–Khalatnikov (HVBK) model (Bekarevich and Khalatnikov, 1961; Hall et al., 1956a,b) describes the normal fluid motion by the NS model, while the superfluid motion is simplified to an Euler-like equation. The two fluids are coupled through a friction force that takes into account the influence of quantized vortices through a coarse-grained averaged superfluid vorticity. The average is considered over an ensemble of parallel (polarized) vortex filaments to find an equivalent solid-body vorticity for a dense vortex bundle of line density. The individual dynamics of quantized vortices thus disappears in the HVBK model.

A different trade-off is made in Line Vortex Navier-Stokes (LV-NS) models. Quantized vortices are described as geometrical lines, with infinite velocity and singular vorticity at the centreline. Vortex lines are moved following the Biot-Savart law and phenomenological models for vortex reconnection are applied. Mutual friction is described, in a more mesoscopic way, by assessing the interaction between the normal NS fluid and the vortex line dynamics (Adachi et al., 2010; Kivotides et al., 2000; Galantucci et al., 2020). These phenomenological LV-NS models typically contain two ingredients. First, on the vortex lines, a **slip velocity** is added to the Biot-Savart line velocity. This slip velocity is obtained as a function of the counterflow (the difference between the normal fluid velocity on the line and the line velocity) by a standard argument based on the balance of friction and Magnus forces. Second, a spatially smoothed **friction force**, opposite to the friction force acting on the line, is added as a source term in the NS equations. These vortex line models are limited with respect to both vortex reconnection (that is added to the model in an ad hoc manner) and to vortex nucleation (that is simply non-existent in these models).

The present contribution is a first attempt, to the best of our knowledge, to directly couple incompressible NS and GP models and thus numerically simulate, without any simplification, the dynamics of a two-fluid quantum flow.

The model is inspired by existing LV-NS models from which we extract the main physical ingredients of the mutual friction produced by the interaction of the normal fluid and superfluid vortices. The novelty is that we transpose this mutual friction coupling into the framework of the GP model that has the advantage to describe vortex nucleation and vortex interactions without any phenomenological assumptions (Koplik and Levine, 1993; Frisch et al., 1992). We develop consistent expressions for the coupling with new interaction terms and we prove numerically that they are compatible with known phenomenological mutual friction laws. We first derive a **regularized line velocity field** that is smooth and reduces to the value of the line velocity, when evaluated on the vortex line. Using this regularized velocity field we build a slip velocity field that is used to couple GP and NS equations. As a main consequence of this study, coupling of NS and GP numerical codes becomes possible with this new GP-NS model.

We should mention that, in the different context of Landau’s original **compressible** two-fluid model (Balibar, 2017) describing second sound and containing neither vortices nor mutual friction, Coste (Coste, 1998) studied ways to couple NS and GP equations. Nevertheless, an outcome of Coste’s model was to introduce a simple coupling law of the local counterflow vector to the GP equation. In the following we will use a coupling that is closely related, but different, to the one pioneered by Coste.

The paper is organized as follows. The theoretical background is given in Section 2. After first defining the uncoupled GPE and NSE equations in Section 2.1 the coupling terms are derived in Section 2.2. The numerical implementation is described in Section 2.3. Our results are contained in Section 3 and, finally, Section 4 is our conclusion.

## 2 Theoretical background

### 2.1 The uncoupled GP and NS equations

The GP equation is a partial differential equation describing the dynamics of a dilute superfluid Bose-Einstein condensate at zero-temperature. It applies to a complex field  $\psi$ , where  $|\psi|^2$  is the number of particles per unit volume, and reads

$$i\hbar\frac{\partial\psi}{\partial t} = -\frac{\hbar^2}{2m}\nabla^2\psi + g|\psi|^2\psi, \quad (1)$$

where  $m$  is the mass of the condensed particles,  $\hbar$  the reduced Planck constant, and  $g$  the interaction constant with  $g = 4\pi\tilde{a}\hbar^2/m$  and  $\tilde{a}$  the  $s$ -wave scattering length.

Equation (1) can be mapped into hydrodynamic equations for a compressible fluid by the Madelung transformation

$$\psi(\mathbf{x}, t) = \sqrt{\frac{\rho(\mathbf{x}, t)}{m}} \exp\left(i\frac{m}{\hbar}\phi(\mathbf{x}, t)\right), \quad (2)$$

where  $\rho(\mathbf{x}, t)$  is the mass density of the fluid,  $\phi(\mathbf{x}, t)$  the velocity potential associated to the fluid velocity  $\mathbf{v} = \frac{\hbar}{m}\nabla\phi$ . This transformation is singular on the zeros of  $\psi$ . As two conditions are required (both real and imaginary parts of  $\psi$  must vanish), these singularities generically take the form of points in 2D and lines in 3D. The Onsager-Feynman quantum of velocity circulation around vortex lines with  $\psi = 0$  is  $\Gamma = h/m$ . Thus, due to the multivalued nature of the velocity potential in the presence of vortex lines, the superflow is not irrotational. It can be proved (Clark di Leoni et al., 2017), using the Madelung transformation, that the vorticity  $\omega = \nabla \times \mathbf{v}$  is given by

$$\omega(\mathbf{r}) = \frac{h}{m} \int ds \frac{d\mathbf{r}_0}{ds} \delta(\mathbf{r} - \mathbf{r}_0(s)), \quad (3)$$

where  $\mathbf{r}_0(s)$  denotes the position of the vortex line,  $\delta$  is the Dirac delta function and  $s$  the arclength. Thus, the vorticity in a quantum flow is a distribution concentrated along the  $\psi = 0$  topological line defects where  $\mathbf{v}$  is ill-behaved (with a  $1/r$  divergence).

Linearizing the GP equation around a constant state  $\psi = \Psi_0$  yields the Bogoliubov dispersion relation for density plane waves ( $\rho_0 e^{i(\mathbf{k}\cdot\mathbf{x} - \omega t)}$ , with  $\mathbf{k}$  the wave number vector):

$$\omega_B(k) = \sqrt{\frac{g\mathbf{k}^2|\Psi_0|^2}{m} + \frac{\hbar^2\mathbf{k}^4}{4m^2}}. \quad (4)$$

The sound velocity is thus given by

$$c = \sqrt{g|\Psi_0|^2/m}. \quad (5)$$

Dispersive effects take place for length scales smaller than the coherence length, defined by

$$\xi = \frac{\hbar}{\sqrt{2gm|\Psi_0|^2}}. \quad (6)$$

Note that  $\xi$  is proportional to the radius of the vortex core (Nore et al., 1997a,b).

The GP equation conserves the total energy  $E$ , the total mass  $\mathcal{M}$ , and the momentum  $\mathbf{P}$ , which are defined in a volume  $V$  as

$$E = \int_V \left( \frac{\hbar^2}{2m} |\nabla\psi|^2 + \frac{g}{2} |\psi|^4 \right) d^3x, \quad (7)$$

$$\mathcal{M} = m \int_V |\psi|^2 d^3x, \quad (8)$$

$$\mathbf{P} = \int_V \frac{i\hbar}{2} (\psi \nabla \bar{\psi} - \bar{\psi} \nabla \psi) d^3x, \quad (9)$$

where the overline denotes the complex conjugate.

To describe the dynamics of a viscous incompressible flow of velocity vector field  $\mathbf{v}$  we use the Navier-Stokes equations

$$\partial_t \mathbf{v} + (\mathbf{v} \cdot \nabla) \mathbf{v} = -\frac{1}{\rho} \nabla p + \nu \nabla^2 \mathbf{v}, \quad (10)$$

$$\nabla \cdot \mathbf{v} = 0, \quad (11)$$

where  $\rho$  is the constant flow density,  $\nu$  the kinematic viscosity and  $p$  denotes the pressure field that enforces incompressibility (*i. e.* zero divergence velocity field).

The NS equations (10)-(11) conserve the total mass and the total momentum and, only for inviscid flows (with  $\nu = 0$ ) the energy is also conserved:

$$E = \rho \int_V \frac{\mathbf{v}^2}{2} d^3x, \quad (12)$$

$$\mathcal{M} = \rho \int_V d^3x, \quad (13)$$

$$\mathbf{P} = \rho \int_V \mathbf{v} d^3x. \quad (14)$$

## 2.2 Building up the model

Our reasoning of model building is the following. In a nutshell, standard phenomenological Line Vortex Navier Stokes (LV-NS) models, such as those developed by [Adachi et al. \(2010\)](#); [Kivotides et al. \(2000\)](#); [Galantucci et al. \(2020\)](#), are based on the argument of cancellation of the sum of mutual friction force and Magnus force acting on the vortex line. The former is caused by the difference between the normal fluid velocity and vortex line velocity, while the latter is caused by the slip velocity, *i. e.* the difference between the vortex line velocity and superfluid velocity. This cancellation yields a phenomenological expression for the slip velocity of the vortex line that is added to the Biot-Savart expression for the equation of motion of the lines. The volume friction force that is added as a source term in the NS equation is then obtained by spatially smoothing the friction on the vortex line.

To apply the same logic to a Gross-Pitaevskii-Navier-Stokes (GP-NS) model, three separate ingredients are needed. The first one is the equivalent of the Biot-Savart velocity of vortex lines: we need a (smooth) field  $\mathbf{v}_s^{reg}$  (obtained from the GP wave function  $\psi$ ) that, when evaluated on vortex lines, will give the line velocities induced by the GP dynamics (in the absence of friction). Second, we need to generalize (using a volume force version) the expression of mutual friction and Magnus force cancellation. This computation will yield two results: (i) a line slip velocity field  $\mathbf{v}_{slip}$  which reduces on the vortex line to the standard expression used in LV-NS models and (ii) a friction force field  $\mathbf{F}_{SN}$  that will be added to the right-hand side of the NS equation. Finally, as a third ingredient, we need an expression for the coupling term in the GP equation that will produce the correct slip velocity  $\mathbf{v}_{slip}$  of vortex lines. This coupling term is closely related, but different, to the one pioneered by [Coste \(1998\)](#).

### 2.2.1 The regularized superfluid velocity field

The superfluid velocity  $\mathbf{v}_s$  can be simply defined by using the superfluid density  $\rho_s = |\psi|^2$  and the relation  $\mathbf{P} = \rho_s \mathbf{v}_s$  for the superfluid momentum, with  $\mathbf{P}$  defined in Eq. (9). However, with line vortices present in the GP model, the associated  $\mathbf{v}_s$  can also be estimated by using the Biot-Savart expression stemming from Eq. (3). Since  $\mathbf{v}_s$  has singularities on the vortex line, we have to introduce a regularized velocity  $\mathbf{v}_s^{reg}$  that is finite on vortex lines and yields the correct velocity circulation at large distances from vortex

lines. To wit, we use the following Gaussian smoothing of the physical space field

$$\begin{aligned}\mathbf{v}_s^\epsilon(\mathbf{r}) &= \frac{i\hbar}{2m} \frac{\psi \nabla \bar{\psi} - \bar{\psi} \nabla \psi}{\bar{\psi} \psi + \epsilon^2 \bar{\rho}_s}, \\ \mathbf{v}_s^{reg} &= (1 + \epsilon^2) \mathcal{F}^{-1} \left( e^{-\frac{k^2}{k_{reg}^2}} \mathcal{F}(\mathbf{v}_s^\epsilon) \right),\end{aligned}\quad (15)$$

where  $\mathcal{F}$  denotes the Fourier transform and  $\bar{\rho}_s = \langle |\psi|^2 \rangle$  is the spatially averaged superfluid density. The smoothing wave-number parameter  $k_{reg}$  is analogous to the smoothing distance used as a parameter in LV-NS models to obtain the volume force added to NS equations. Parameter  $\epsilon$  is used to avoid velocity divergence on the vortex line (where  $\bar{\psi} \psi = 0$ ) and has to be large enough to correctly resolve vortex lines. In practice (see Section 2.3), we set  $\epsilon^2 = 0.1$  and  $k_{reg} = 1/\xi$ .

The regularised velocity field allows one to define a smoothed vorticity, as the curl of the regularized velocity:

$$\boldsymbol{\Omega} = \nabla \times \mathbf{v}_s^{reg}. \quad (16)$$

For a straight vortex line, the effect of this Gaussian smoothing on the maximum value of smoothed vorticity, can be estimated to be  $F^{-1}$ , given by the integral

$$F^{-1} = \frac{\hbar}{2m} \frac{1}{\pi} \left[ \int_{-\infty}^{\infty} e^{-\frac{k^2}{k_{reg}^2}} dk \right]^2 = \frac{\hbar}{2m} k_{reg}^2. \quad (17)$$

We finally define the 'normalized' vorticity field

$$\hat{\boldsymbol{\Omega}} = F \boldsymbol{\Omega} = F \nabla \times \mathbf{v}_s^{reg}, \quad (18)$$

which has a norm that is maximum and close to 1 on the vortex line and much smaller than 1 away from the vortex line.

### 2.2.2 Determination of the slip velocity field and volume friction force

The Magnus force density caused by  $\mathbf{v}_{slip}$  can be estimated starting from the momentum conservation equation (Sonin, 1997):

$$\mathbf{F}_{MD} = \rho_s \mathbf{v}_{slip} \times (\nabla \times \mathbf{v}_s^{reg}). \quad (19)$$



This force density must be opposite to the force density acting on the NS fluid, thus

$$\mathbf{F}_{MD} = -\mathbf{F}_{SN}. \quad (20)$$

For  $\mathbf{F}_{SN}$  we start from the simple phenomenological expression considering a force with longitudinal and transversal components

$$\mathbf{F}_{SN} \sim \rho_n [\beta s' \times (s' \times (\mathbf{v}_n - \mathbf{v}_L)) + \beta' s' \times (\mathbf{v}_n - \mathbf{v}_L)], \quad (21)$$

where  $\rho_n$  and  $\mathbf{v}_n$  are the density and velocity of the normal fluid,  $\mathbf{v}_L$  the velocity of the vortex line,  $s'$  the unit tangent to the line (see Fig. 1), and  $\beta$ ,  $\beta'$  two phenomenological coefficients.

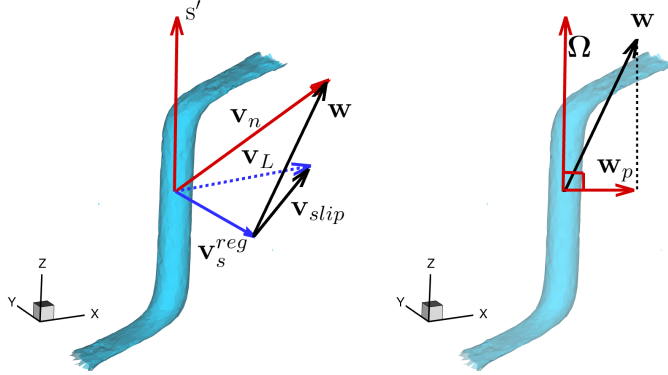


Figure 1: Sketch of velocities acting on a vortex line.

Using the fact that **on vortex lines** the vector  $\hat{\Omega} = F\Omega$  is of norm 1 and directed along the line, we postulate the following formula for the volume force, equivalent to Eq. (21):

$$\mathbf{F}_{SN} = \rho_n [B_\star (\nabla \times \mathbf{v}_s^{reg}) \times (F(\nabla \times \mathbf{v}_s^{reg}) \times (\mathbf{v}_n - \mathbf{v}_L)) + B'_\star (\nabla \times \mathbf{v}_s^{reg}) \times (\mathbf{v}_n - \mathbf{v}_L)], \quad (22)$$

with  $B_\star$  and  $B'_\star$  the new phenomenological constants. After replacing in (20) the expressions (19) and (22), we need to solve

$$0 = -\rho_s (\nabla \times \mathbf{v}_s^{reg}) \times \mathbf{v}_{slip} + \rho_n [B_\star (\nabla \times \mathbf{v}_s^{reg}) \times (F(\nabla \times \mathbf{v}_s^{reg}) \times (\mathbf{v}_n - \mathbf{v}_L)) + B'_\star (\nabla \times \mathbf{v}_s^{reg}) \times (\mathbf{v}_n - \mathbf{v}_L)]. \quad (23)$$

Because of the coupling induced slip velocity, the line velocity  $\mathbf{v}_L$  is given by (see Fig. 1)

$$\mathbf{v}_L = \mathbf{v}_s^{reg} + \mathbf{v}_{slip}. \quad (24)$$

Therefore (23) becomes

$$\begin{aligned} 0 = & -\rho_s (\nabla \times \mathbf{v}_s^{reg}) \times \mathbf{v}_{slip} \\ & + \rho_n [B_\star (\nabla \times \mathbf{v}_s^{reg}) \times (F(\nabla \times \mathbf{v}_s^{reg}) \times (\mathbf{v}_n - \mathbf{v}_s^{reg} - \mathbf{v}_{slip})) \\ & + B'_\star (\nabla \times \mathbf{v}_s^{reg}) \times (\mathbf{v}_n - \mathbf{v}_s^{reg} - \mathbf{v}_{slip})]. \end{aligned} \quad (25)$$

A general remark on the equation to solve for  $\mathbf{v}_{slip}$  is that it involves two vectors fields that are obtained from the normal and superfluid components: the counterflow (see Fig. 1)

$$\mathbf{w} = \mathbf{v}_n - \mathbf{v}_s^{reg}, \quad (26)$$

and the (regularized) superfluid vorticity  $\mathbf{\Omega}$  defined in (16). Recall that  $\mathbf{\Omega}$  is aligned, on vortex lines, to the vector  $s'$  tangent to the line. Supposing that  $\mathbf{w}$  is not aligned with  $\mathbf{\Omega}$ , we define the component of  $\mathbf{w}$  perpendicular to the vortex line (see Fig. 1)

$$\mathbf{w}_p = \mathbf{w} - \frac{\mathbf{w} \cdot \mathbf{\Omega}}{\mathbf{\Omega} \cdot \mathbf{\Omega}} \mathbf{\Omega}. \quad (27)$$

We note that a natural vector basis is then  $(\mathbf{\Omega}, \mathbf{w}_p, \mathbf{\Omega} \times \mathbf{w})$ .

Using these variables, Eq. (25) becomes

$$0 = -\rho_s \mathbf{\Omega} \times \mathbf{v}_{slip} + \rho_n [B_\star \mathbf{\Omega} \times (F \mathbf{\Omega} \times (\mathbf{w} - \mathbf{v}_{slip})) + B'_\star \mathbf{\Omega} \times (\mathbf{w} - \mathbf{v}_{slip})], \quad (28)$$

which is the same as

$$0 = -\rho_s \mathbf{\Omega} \times \mathbf{v}_{slip} + \rho_n [B_\star \mathbf{\Omega} \times (F \mathbf{\Omega} \times (\mathbf{w}_p - \mathbf{v}_{slip})) + B'_\star \mathbf{\Omega} \times (\mathbf{w}_p - \mathbf{v}_{slip})]. \quad (29)$$

After some elementary algebraic manipulations (see details in A), we obtain closed expressions for the mutual friction, the Magnus force and the slip velocity  $\mathbf{v}_{slip}$ . The latter is presented in the following convenient form

$$\mathbf{v}_{slip} = U_\star \mathbf{w}_p + V_\star \hat{\mathbf{\Omega}} \times \mathbf{w}, \quad (30)$$

with  $\hat{\mathbf{\Omega}}$  defined in (18) and

$$U_\star = \frac{\rho_n (B_\star^2 |\hat{\mathbf{\Omega}}|^2 \rho_n + B'_\star (\rho_s + \rho_n B'_\star))}{B_\star^2 |\hat{\mathbf{\Omega}}|^2 \rho_n^2 + (\rho_s + \rho_n B'_\star)^2}, \quad (31)$$

$$V_\star = \frac{B_\star \rho_n \rho_s}{B_\star^2 |\hat{\mathbf{\Omega}}|^2 \rho_n^2 + (\rho_s + \rho_n B'_\star)^2}. \quad (32)$$

Note that the dimensions of the fields in the above expressions are (with  $L$ ,  $T$  and  $M$  denoting units of length, time and mass):  $[\mathbf{v}_{\text{slip}}] = LT^{-1}$ ;  $[\mathbf{\Omega}] = [\nabla \times \mathbf{v}_s^{\text{reg}}] = T^{-1}$ ;  $[F] = T$ , thus  $[\hat{\mathbf{\Omega}}] = 1$  and  $[\rho] = ML^{-3}$ . In Eq. (19),  $\mathbf{F}_{MD}$  is a force per volume:  $[\mathbf{F}_{MD}] = ML^{-2}T^{-2}$ . The same dimension is obtained in Eq. (22) for  $\mathbf{F}_{SN}$  because of (20):  $[\mathbf{F}_{SN}] = ML^{-2}T^{-2}$ . By inspection, we conclude that the following coefficients are dimensionless:  $B_\star$ ,  $B'_\star$ ,  $U_\star$ ,  $V_\star$ .

To summarize our results,  $\mathbf{v}_{\text{slip}}$  is obtained from (30)-(31)-(32) and the final expression of the friction force results from (20), (19) and (22) as

$$\mathbf{F}_{SN} = \rho_s \mathbf{\Omega} \times (U_\star \mathbf{w}_p + V_\star \hat{\mathbf{\Omega}} \times \mathbf{w}). \quad (33)$$

### 2.2.3 Definition of coupling terms in the GP equation

Expression (33) gives the smooth friction force field to be added to the right-hand side of the NS momentum equation (10). It is apparent by inspection that the  $U_\star$  term corresponds to a force normal to the counterflow  $\mathbf{w}$  and to a slip velocity parallel to  $\mathbf{w}$ , while the  $V_\star$  term corresponds to a force parallel to  $\mathbf{w}$  and a slip velocity perpendicular to  $\mathbf{w}$ . Therefore, on physical grounds, we expect the  $V_\star$  term to remove energy from the GP dynamics (and transfer it to the NS flow) while the  $U_\star$  term is expected just to change the longitudinal speed of a vortex. This point will be important in our definition of the GP coupling term.

We still need to find a way to implement the slip velocity (30) into the GP equation (1) in a way that will make the vortex lines move with an additional velocity  $\mathbf{v}_{\text{slip}}$ . For this purpose, we consider the vortex solution of the stationary GP equation (Nore et al., 1997). In 2D polar coordinates ( $x = r \cos(\theta)$ ,  $y = r \sin(\theta)$ ) this solution representing a positive or negative vortex placed at the origin is

$$\psi_v = R(r)e^{\pm i\theta}, \quad (34)$$

and satisfies

$$0 = -\frac{\hbar^2}{2m} \nabla^2 \psi_v + g|\psi_v|^2 \psi_v. \quad (35)$$

The time-evolution of this vortex advected by a constant vector field  $\mathbf{U}^{adv}$  is described by the partial differential equation

$$\partial_t \psi + \mathbf{U}^{adv} \cdot \nabla \psi = i \left( \frac{\hbar}{2m} \nabla^2 \psi - \frac{g}{\hbar} |\psi|^2 \psi \right), \quad (36)$$

with solution

$$\psi(\mathbf{r}, t) = \psi_v(\mathbf{r} - t\mathbf{U}^{adv}). \quad (37)$$

Consider now the advection velocity

$$\mathbf{U}_{\perp}^{adv} = \pm \hat{\mathbf{e}}_z \times \mathbf{U}^{adv}, \quad (38)$$

where  $\hat{\mathbf{e}}_z$  denotes the unit vector in the  $z$  direction, and the imaginary-time dynamics

$$\partial_t \psi - i\mathbf{U}_{\perp}^{adv} \cdot \nabla \psi = i \left( \frac{\hbar}{2m} \nabla^2 \psi - \frac{g}{\hbar} |\psi|^2 \psi \right). \quad (39)$$

Setting  $\mathbf{U}^{adv} = (\cos(\theta^{adv}), \sin(\theta^{adv}))$  and using space and time Taylor series expansions in both positive and negative vortex cases, the vortex position  $(\delta x, \delta y)$  for short times  $\delta t$  is given by the solution of the equation

$$(\delta x + i\delta y - e^{i\theta^{adv}} \delta t) \frac{dR}{dr}(0) = 0, \quad (40)$$

showing that the position of the vortex is indeed moving with velocity  $\mathbf{U}^{adv}$ .

Thus, there are two different ways to move vortex lines in the GP framework with real advection velocity  $\mathbf{U}^{adv}$ , by adding a term which is either real (36) or imaginary (39).

The first approach (36) corresponds to that suggested by Coste (1998) and is best suited for non-dissipative processes of the GP type. Coste (1998) coupled a vector  $\mathbf{v}$  field to GP dynamics (1) through the following substitutions

$$\nabla \rightarrow \nabla + \frac{i}{2\alpha} \mathbf{v}, \quad (41)$$

where we used the short-hand notation  $\alpha = \frac{\hbar}{2m}$ . The new gradient is similar to the covariant gradient  $\nabla + i\mathbf{A}$  used in magnetic Ginzburg-Landau models, with  $\mathbf{A}$  the electro-magnetic potential vector field (Sandier and Serfaty, 2007). We notice that

$$\alpha \nabla^2 \rightarrow \alpha \nabla^2 + i\mathbf{v} \cdot \nabla + \frac{i}{2} (\nabla \cdot \mathbf{v}) - \frac{\mathbf{v}^2}{4\alpha}, \quad (42)$$

where the divergence term in the right-hand side of (42) enforces mass conservation in the modified GP equation, which becomes

$$-i\partial_t \psi = \alpha \nabla^2 \psi + i\mathbf{v} \cdot \nabla \psi + \frac{i}{2} (\nabla \cdot \mathbf{v}) \psi - \frac{\mathbf{v}^2}{4\alpha} \psi - \frac{g}{\hbar} |\psi|^2 \psi. \quad (43)$$

Note that, for constant  $\mathbf{v}$ , this is a simple Galilean boost with speed  $\mathbf{v}$ . Indeed, recall that the Galilean invariance of the GP equation explicitly reads:

$$\psi(\mathbf{x}, t) \rightarrow \psi(\mathbf{x} - \mathbf{U}^{adv}t, t) \exp\left(i\left(\frac{\mathbf{U}^{adv}}{2\alpha} \cdot \mathbf{x} - \frac{(\mathbf{U}^{adv})^2}{4\alpha}t\right)\right), \quad (44)$$

where  $\mathbf{U}^{adv}$  is the constant velocity of the boost. This transformation maps any solution  $\psi(\mathbf{x}, t)$  of the GP equation into another solution with associated velocity and density fields that are Galilean transforms of those associated to  $\psi$ . Thus, with  $\psi_v(\mathbf{x})$  denoting as before a time-stationary vortex line solution of the GP equation, the initial data  $\psi_v(\mathbf{x}) \exp(i\frac{\mathbf{U}^{adv}}{2\alpha} \cdot \mathbf{x})$  corresponds to a vortex translating with (uniform) velocity  $\mathbf{U}^{adv}$ .

The second approach (39) is new and related to the damped Schrödinger/Gross-Pitaevskii equation (Bao and Cai, 2013), introducing a dissipative dynamics of the Ginzburg-Landau type. Nore et al. (1997a) prepared an initial data for the GP equation consisting of an array of vortex lines moving at short times with given large-scale velocity field  $\mathbf{U}^{adv}$  by finding a stationary solution of the Advective Real Ginzburg-Landau Equation (ARGLE):

$$\partial_t \psi = \alpha \nabla^2 \psi + (\bar{\rho}_s - \frac{g}{\hbar} |\psi|^2) \psi - i \mathbf{U}^{adv} \cdot \nabla \psi - \frac{(\mathbf{U}^{adv})^2}{4\alpha} \psi. \quad (45)$$

A solution to (45) corresponds to a minimum of the associated (modified) GP energy functional:

$$\mathcal{E}_{ARGLE}[\psi, \bar{\psi}] = \int \left( \alpha \left| \nabla \psi - i \frac{\mathbf{U}^{adv}}{2\alpha} \psi \right|^2 + \left( \frac{g}{2} |\psi|^4 - |\psi|^2 \right) \right) d^3x. \quad (46)$$

We note that the advection term in the ARGLE Eq. (45) has opposite sign to the advection term in (39). This means, heuristically, that in an ARGLE-converged stationary state with vortices, the motion that would be created by all vortices is equally balanced by the ARGLE advection term.

Based on these mathematical-physical observations, we conclude that is necessary to split the slip velocity  $v_{slip}$ , defined in Eq. (30), into  $v_{slip}^{\parallel} = U_{\star} \mathbf{w}_p$  and  $v_{slip}^{\perp} = V_{\star} \hat{\boldsymbol{\Omega}} \times \mathbf{w}$ . For the coupling with GP equation we use the approach (36) with  $\mathbf{U}^{adv} = v_{slip}^{\parallel}$  and (39) with  $\mathbf{U}_{\perp}^{adv}$  given by (38). Note that in our case  $\mathbf{U}_{\perp}^{adv} = \pm (\pm \frac{\hat{\boldsymbol{\Omega}}}{|\hat{\boldsymbol{\Omega}}|}) \times (V_{\star} \hat{\boldsymbol{\Omega}} \times \mathbf{w}) = V_{\star} |\hat{\boldsymbol{\Omega}}| \mathbf{w}_p$ .

Finally, the expression that has to be used for  $\mathbf{v}$  in the modified GP equation (43) is

$$\mathbf{v}_{slip}^{cpl} = (U_{\star} + i V_{\star} |\hat{\boldsymbol{\Omega}}|) \mathbf{w}_p. \quad (47)$$

Implemented in this way, the coupling corresponding to the perpendicular speed dissipates energy, as it should be, because of the work of the friction force.

### 2.3 Numerical coupling algorithm

We start by solving the modified Navier-Stokes equations written in the form:

$$\begin{aligned}\partial_t \mathbf{v}_n + (\mathbf{v}_n \cdot \nabla) \mathbf{v}_n &= -\frac{1}{\rho_n} \nabla p + \nu_n \nabla^2 \mathbf{v}_n + \frac{1}{\rho_n} \mathbf{F}_{SN}, \\ \nabla \cdot \mathbf{v}_n &= 0,\end{aligned}\tag{48}$$

where

$$\mathbf{F}_{SN} = \rho_s (\nabla \times \mathbf{v}_s^{reg}) \times (U_\star \mathbf{w}_p + V_\star \hat{\Omega} \times \mathbf{w}),\tag{49}$$

with  $\mathbf{w} = \mathbf{v}_n - \mathbf{v}_s^{reg}$ ,  $\mathbf{w}_p = \mathbf{w} - \frac{\mathbf{w} \cdot \hat{\Omega}}{|\hat{\Omega}|^2} \hat{\Omega}$  and  $U_\star$  and  $V_\star$  given by Eqs. (31) and (32), respectively. Fields  $\mathbf{v}_s^{reg}$  and  $\hat{\Omega}$  given by Eq. (15) and (18), respectively, realize the coupling with the modified GP equation (43) in which  $\mathbf{v} = \mathbf{v}_{slip}^{cpl}$  from Eq. (47).

A last ingredient is necessary for the coupling model. Given that the normal fluid is assumed incompressible and that the hydrodynamic analogy of the GP equation gives a compressible fluid, we need to ensure the compatibility of the two flows and thus damp acoustic density waves in the GP flow. A standard model is the so-called damped Gross-Pitaevskii equation (Tsubota et al., 2017) using a dissipation term controlled by a small dimensionless parameter  $\eta_D$ . We thus use the following final modified GP equation:

$$\begin{aligned}\partial_t \psi &= i \left( \alpha \nabla^2 \psi - \gamma (|\psi|^2 - \bar{\rho}_s) \psi - \frac{1}{\alpha} \frac{(\mathbf{v}_{slip}^{cpl})^2}{4} \psi \right) \\ &- (\mathbf{v}_{slip}^{cpl} \cdot \nabla) \psi - \frac{1}{2} (\nabla \cdot \mathbf{v}_{slip}^{cpl}) \psi \\ &+ \eta_D (\alpha \nabla^2 \psi - \gamma (|\psi|^2 - \bar{\rho}_s) \psi + \mu \psi).\end{aligned}\tag{50}$$

Parameters  $\alpha = \frac{\hbar}{2m}$  and  $\gamma = \frac{g}{\hbar}$  are determined as usually from  $c$  (see Eq. (5)) and  $\xi$  (see Eq. (6)), with  $|\Psi|_0^2 = \bar{\rho}_s$ . Note that the value of  $\alpha$  should be of order of the normal viscosity  $\nu_n$ . The initial-data wavefunction is normalized to  $|\psi|^2 = \bar{\rho}_s$ . The term  $\mu$  is introduced to ensure mass conservation in the modified GP equation.

The final system of coupled equations (48) and (50) is advanced in time using a fourth-order Runge-Kutta method (with implicit discretization of Laplacian operators). Fourier-spectral space discretization is used for both equations. The coupling algorithm was implemented in the framework of the modern parallel (MPI-OpenMP) numerical code called GPS (Gross-Pitaevskii Simulator) (Parnaudeau et al., 2015). The GPS code was initially designed as a spectral parallel solver for the GP equation using various time-integration methods (Strang splitting, relaxation, Crank-Nicolson). It was recently used to simulate quantum turbulent flows (Kobayashi et al., 2021). The Navier-Stokes solver was added to the GPS code using standard Fourier pseudo-spectral method (Gottlieb and Orszag, 1977). Only one external library, FFTW (Frigo and Johnson, 2005), was required for the computation.

The coupling model has several coefficients that have to be fixed accordingly to the physics or be adjusted numerically. To give the model a physical background, the friction coefficients  $U_\star$  and  $V_\star$  were linked to tabulated experimental friction coefficients  $B_{tab}$  and  $B'_{tab}$  used in the physical literature for helium II. Equivalence relations between friction coefficients are detailed in B. In the following, we prefer to set test cases using realistic values for  $B_{tab}$  and  $B'_{tab}$ . Normal  $\rho_n$  and superfluid  $\rho_s$  mass densities, the normal fluid viscosity  $\nu_n$  are also fixed based on the physics of helium II, depending on the intermediate temperature between 0 and 2.17 K.

The model also includes a few numerical coefficients that have to be prescribed. These extra coefficients are the two smoothing parameters  $\epsilon^2$  and  $k_{reg}$  used in the definition of  $\mathbf{v}_s^{reg}$  (15), and the dissipation coefficient  $\eta_D$  in (50). On dimensional grounds,  $\epsilon^2$  has to be proportional to  $\bar{\rho}_S$ ,  $k_{reg}$  to  $\xi^{-1}$  (the inverse of the healing length) and  $\eta_D$  to the physical friction coefficient  $B_{tab}$ . Remembering that  $\bar{\rho}_S$  is close to the value 1, it is consistent to use  $\epsilon^2 = C_\epsilon \bar{\rho}_S$ , with  $C_\epsilon$  a small value constant. We set the second coefficient in a similar way,  $k_{reg} = C_k \xi^{-1}$ , with  $C_k \leq 1$  (as commonly set in simulations of GP quantum turbulence). The values of constants  $C_\epsilon$  and  $C_k$  will be adjusted in the next section by numerical tests reproducing the evolution of quantized vortices in a normal fluid.

### 3 Numerical results

We use in this section classical cases of vortex dynamics to numerically validate the model. We adopt the following methodology:

- The first preliminary test is more qualitative and intended to check that the coupling model produces the correct displacement of a stationary 2D quantized vortex array. The vortex crystal defined by Nore et al. (1994) is formed by two positive and two negative vortices in a 2D domain  $[0, 2\pi]^2$ , with center coordinates  $(\frac{\pi}{2}, \frac{\pi}{2})$  and  $(\frac{3\pi}{2}, \frac{3\pi}{2})$  for the positive ones, and  $(\frac{3\pi}{2}, \frac{\pi}{2})$  et  $(\frac{\pi}{2}, \frac{3\pi}{2})$  for the negative vortices. This symmetric crystal arrangement has the property that  $\mathbf{v}_s^{\text{reg}} = 0$ , and consequently  $\mathbf{v}_L = \mathbf{v}_{\text{slip}}$  (see Fig. 1). After obtaining the initial state of the crystal by solving the ARGLE equation (45) with  $\mathbf{U}^{adv} = 0$ , it is possible to impose a constant velocity  $\mathbf{v}_n$  to the normal fluid (i.e. the Navier-Stokes equations are not solved) and monitor how the crystal is deformed. For  $\mathbf{v}_n$  directed following the  $x$ -axis the crystal remains stable and is translated by  $\mathbf{v}_{\text{slip}}$ , while for vertical  $\mathbf{v}_n$ , the crystal is deformed and a superfluid velocity  $\mathbf{v}_s^{\text{reg}}$  appears. The obtained short term behavior (pictures not shown) of the vortex crystal corresponds to this expected motion and thus confirms that the coupling model gives the correct displacement of quantized vortices in an imposed constant normal flow.
- The second numerical test is aimed at finely tune the parameters of the model ( $\epsilon^2$ ,  $k_{\text{reg}}$  and  $\eta_D$ ) for a vortex configuration with non-trivial  $\mathbf{v}_s^{\text{reg}}$ . For this purpose, we use the case of a 2D vortex dipole for which analytical solutions are available. The one- or two-way GP-NS coupling could be tested using this benchmark. This case is described in detail in Sec. 3.1.
- Once the values of the parameters are fixed, we test the complete coupling model by simulating the 3D dynamics of a superfluid vortex ring moving in a normal fluid. We then compare the results with those obtained by LV-NS coupling methods. We describe in Sec. 3.2 the case of a single vortex ring and the case of the head-on collision of two vortex rings, moving in a normal fluid.



### 3.1 2D superfluid vortex dipole and determination of model coefficients

We consider a superfluid vortex dipole in a periodic domain  $[0, 2\pi]^2$ . The positive vortex (of circulation  $\Gamma = \frac{h}{m} = 4\pi\alpha$ ) is initially centered at  $(x_+, y_+) = (x_0, \pi + \frac{R_0}{2})$  and the negative vortex (of circulation  $-\Gamma$ ) at  $(x_-, y_-) = (x_0, \pi - \frac{R_0}{2})$ . The dipole is moving along the  $x$ -axis, symmetrically to the center line  $y = \pi$ . Parameters  $x_0$  and  $R_0$  define the initial streamwise position of the dipole and its initial radius, respectively. In absence of normal fluid, the superfluid dipole translates in a periodic domain with known velocity (Griffin et al., 2020):

$$\mathbf{u}_s = u_s \mathbf{e}_x, \quad u_s \approx \frac{\Gamma}{4\pi} \left( \frac{1 + \cos(d)}{\sin(d)} + \frac{d}{\pi} \right), \quad (51)$$

where  $d = 2R = y^+ - y^-$  is the distance between vortices. If a constant normal fluid velocity is imposed along the streamwise direction ( $\mathbf{u}_n = u_n \mathbf{e}_x$ ), the balance of forces acting on the dipole lead to the following analytical expressions for the horizontal  $\dot{x}(t)$  and vertical  $\dot{R}(t)$  velocities describing the dynamics of the dipole (see details in C):

$$\dot{x}(t) = \frac{\gamma_0^2 \rho_s \omega_s (u_n - u_s)}{(\gamma_0^2 + (\gamma_0' - \rho_s \omega_s)^2)(\rho_s \omega_s - \gamma_0')} + \frac{u_s \rho_s \omega_s - \gamma_0' u_n}{\rho_s \omega_s - \gamma_0'}, \quad (52)$$

$$\dot{R}(t) = \frac{\gamma_0 \rho_s \omega_s}{\gamma_0^2 + (\gamma_0' - \rho_s \omega_s)^2} (u_n - u_s), \quad (53)$$

where  $\gamma_0, \gamma_0'$  are two physical parameters related to the temperature and  $\omega_s = (\nabla \times \mathbf{u}_s) \mathbf{e}_z$ . Solution (52)-(53) is used in the following to finely tune the parameters of the coupling model.

#### 3.1.1 One-way GP-NS coupling

We start by considering the one-way GP-NS coupling. The NS equations are not solved and we take  $u_n = 0$ , which gives simpler relations for the analytical solution (52)-(53). The superfluid vortex dipole is initially generated using the method suggested by Billam et al. (2014) to impose the atomic density and the phase of the wave function. This case allows us to assess on the effect of the three parameters of the model:

- The *regularization wave-number*  $k_{\text{reg}}$  is necessary in Eq. (15) to obtain a smooth velocity  $\mathbf{v}_s^{\text{reg}}$  and corresponding smooth vorticity  $\mathbf{\Omega}$  in Eq. (16).

It acts like a filter by smoothing the superfluid velocity and slightly diffusing the vorticity in the surrounding area of a vortex, which is the zone where the coupling force term is computed. The choice of the regulation length scale  $1/k_{\text{reg}}$  was found to be critical to balance the accuracy and validity of the numerical simulation. If  $k_{\text{reg}}$  is too large (i. e. the vorticity around a vortex line is not smooth enough), the results could be more accurate, but the simulation might be unstable because of numerical oscillations (wiggles). On the other hand, if  $k_{\text{reg}}$  is too small, the numerical results are stable, but the accuracy is diminished. A trade-off between these two effects thus should be found. Figure 2 (a) shows that by decreasing  $k_{\text{reg}}$ , the vortices of the dipole approach to each other with an increasing rate. We fixed  $k_{\text{reg}} = 1/\xi$ , considering that a regularization length scale of the order the vortex core is physically reasonable.

- The *small parameter*  $\epsilon^2$  in Eq. (15) is also needed to avoid the singularity of the superfluid velocity when the vortex line pass near a mesh node (as  $\bar{\psi}\psi$  is zero on the vortex line). We took  $\epsilon^2 = 0.1$  to ensure that the corresponding effective regularization length  $0.31\xi$  is smaller than regularization length introduced by the  $k_{\text{reg}}$ .
- The *dissipation* parameter  $\eta_D$  was introduced in the GP equation to damp sound (pressure) waves and thus ensure the compatibility of the model with the incompressible flow assumption for both normal and superfluid. This dissipation effect is also affecting the intensity of the coupling force, which suggests that is reasonable to assume that  $\eta_D$  is proportional to  $B_{tab}$ . Figure 2 (b) compares the numerical results with the analytical solution with different  $\eta_D$ . When setting  $\eta_D = 0$ , we found that the two vortices of the dipole do not approach to each other fast enough and the gap between their positions do not evolve any more after reaching the value of approximately  $10\xi$ . When  $\eta_D$  is increased, vortices approach to each other in a increasing rate. The parameter  $\eta_D$  was finally fixed to the value  $0.02B_{tab}$ , for which the numerical solution fits perfectly to the analytical solution. When  $B_{tab} = B'_{tab}$ , the value  $\eta_D = 0.01B_{tab}$  is also a good choice for the dissipation constant.

Figure 2 (c) shows that using the values  $\epsilon^2 = 0.1$ ,  $k_{\text{reg}} = 1/\xi$  and  $\eta_D = 0.02B_{tab}$ , the numerical results fit perfectly with the analytical solution for different coupling force coefficients  $B_{tab}$  and  $B'_{tab}$ . Figure 3 offers a final

validation of the values found for the parameters of the model by depicting the time trajectories and time evolution of the radius of the dipole for typical values of coupling force coefficients  $B_{tab} = 0.4$  and  $B'_{tab} = 0.1$  (that will be used in the next sections).

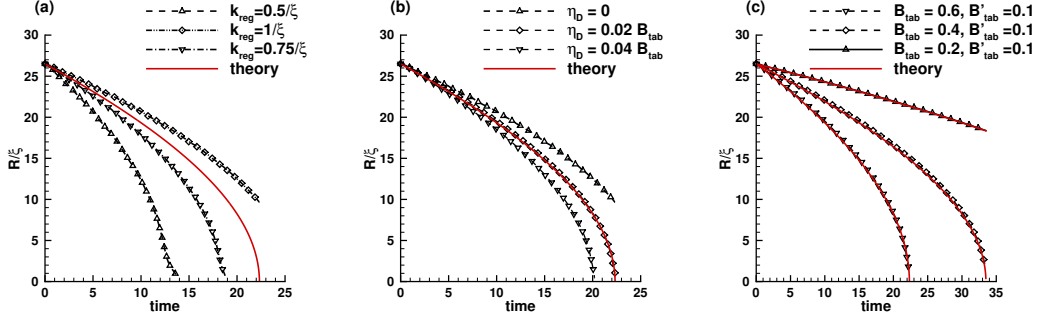


Figure 2: 2D evolution of a superfluid vortex dipole. One-way GP-NS coupling, with  $\mathbf{u}_n = 0$ . Time evolution of the half distance between the two vortices normalized by the size of the vortex core  $\xi$ . Solid lines represent the analytical solution. (a) Results for three values of the smoothing wave number  $k_{reg}$  and common values  $B_{tab} = 0.6$  and  $B'_{tab} = 0.1$ . (b) Results for three values of the dissipation parameter  $\eta_D$  and common values  $B_{tab} = 0.6$  and  $B_{tab} = 0.1$ . (c) Results for  $k_{reg} = 1/\xi$ ,  $\eta_D = 0.02 B_{tab}$ , and three different choices for the coupling force parameters  $B_{tab}$  and  $B'_{tab}$ .

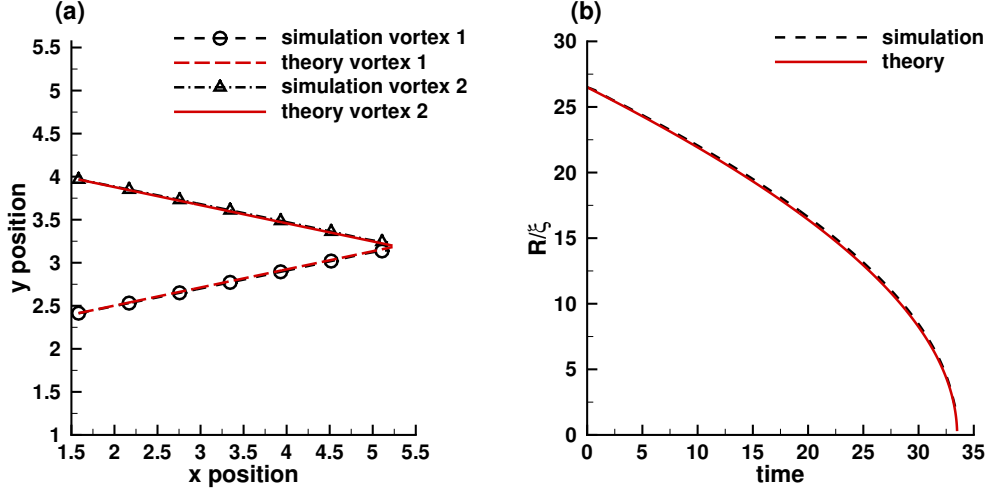


Figure 3: 2D evolution of a superfluid vortex dipole. One-way GP-NS coupling, with  $\mathbf{u}_n = 0$ . Simulation with fixed parameters:  $B_{tab} = 0.4$ ,  $B'_{tab} = 0.1$ ,  $d/\xi = 53$ ,  $N = 256$ ,  $k_{reg}^{-1} = \xi$ ,  $\eta_D = 0.02B_{tab}$ . (a) Trajectories of the two vortices. (b) Time evolution of the the half distance between the two vortices normalized by the size of the vortex core.

### 3.1.2 Two-way GP-NS coupling

We now simulate the time evolution of the same 2D dipole, but with the full two-way GP-NS coupling. The parameters of the model are kept the same as determined from the one-way coupling. The difference between the two types of coupling is visible in Fig. 4. When considering the coupling force in the NS equations (two-way coupling), the vortices of the dipole approach to each other with a reduced rate. This was expected, since the moving vortex dipole generates, through the coupling force, a normal fluid velocity ( $u_n \neq 0$ ) that finally counteracts the mutual friction. The configuration of the flow is illustrated in Fig. 5 presenting snapshots of the normal fluid vorticity and streamlines, together with the identification of the superfluid vortices by iso-contours of low-atomic density. We observe a *triple-vortex-pair* structure consisting of a pair of superfluid anti-vortex and two pairs of anti-vortex of normal fluid: the first one is surrounding the superfluid vortices and rotates in the same direction, and the second one is adjacent to superfluid vortices and rotates in the opposite direction. The stream lines show how the normal

fluid is entrained by the motion of the superfluid vortex pair. By comparing the two snapshots, we can also observe that vortices move towards each other while translating downstream.

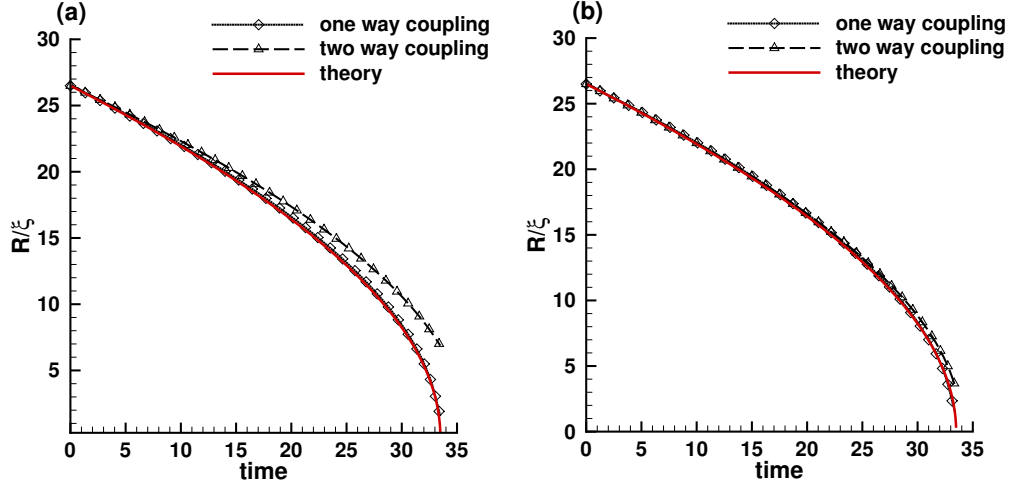


Figure 4: 2D evolution of a superfluid vortex dipole. Time evolution of the half distance between the two vortices normalized by the size of the vortex core  $\xi$ . Comparison between  $(-\diamond-)$  one-way coupling ( $\mathbf{u}_n = 0$ ) and  $(-\triangle-)$  two-way coupling ( $\mathbf{u}_n \neq 0$ ) for different physical parameters (a) :  $B_{tab} = 0.4$ ,  $B'_{tab} = 0.1$ ,  $\eta_D = 0.02B_{tab}$ , (b) :  $B_{tab} = 0.4$ ,  $B'_{tab} = 0.4$ ,  $\eta_D = 0.01B_{tab}$ . Common parameters of the model:  $d/\xi = 53$ ,  $N = 256$ ,  $k_{reg}^{-1} = \xi$ .

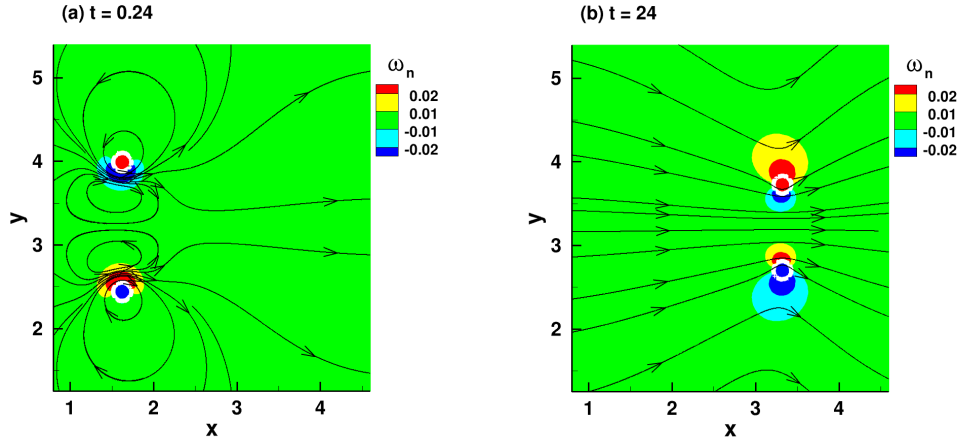


Figure 5: 2D evolution of a superfluid vortex dipole. Two-way GP-NS coupling. Illustration of the triple-vortex structure of the flow. The entrained normal fluid is represented by its vorticity contours (colors) and streamlines (arrow black lines). Superfluid vortices (white circles) are identified by an iso-contour of low atomic density ( $0.5 |\psi|_{max}^2$ ). Snapshots of the flow for time instants: (a)  $t=0.24$ , (b)  $t=24$ . Parameters of the simulation:  $B_{tab} = 0.4$ ,  $B'_{tab} = 0.1$ ,  $\eta_D = 0$ ,  $d/\xi = 53$ ,  $N = 256$ ,  $k_{reg}^{-1} = \xi$ .

## 3.2 3D superfluid vortex ring

The triple-vortex structure observed in the 2D simulation of a vortex dipole is similar to that observed in the 3D flow generated by a superfluid vortex ring moving in a normal fluid (Kivotides et al., 2000; Galantucci et al., 2020; Inui and Tsubota, 2021). We use this case to validate in 3D our full coupling GP-NS coupling model. The initial superfluid vortex ring is generated using Padé approximations and the ARGLE procedure (Kobayashi et al., 2021). The normal fluid is initially at rest.

Figure 6 shows snapshots of the time evolution of the vortex ring for different physical parameters  $B_{tab} = B'_{tab}$  (panels a, b) and  $B_{tab} > B'_{tab}$  (panels c, d). The superfluid vortex ring (in black) moves in the  $x$ -direction from left to right and sweeps surrounding normal fluid due to the action of the coupling force. Two normal fluid vortex rings with opposite circulations are thus created, an outer one with large radius (in blue) and an inside smaller vortex ring (in red). The overall dimension of this triple-vortex rings structure reduces while moving downstream. We thoroughly investigated the influence of the values of physical parameters on the topology of the triple-vortex. When  $B_{tab} \approx B'_{tab}$  the small inner normal vortex ring (in red) travels at the rear of superfluid ring, while for  $B_{tab} > B'_{tab}$  it is placed slightly in front of the superfluid ring.

The triple-vortex ring structure illustrated in Fig. 6 is very similar to that recently found by LV-NS coupling models using vortex filaments for the superfluid and different NS solvers for the normal fluid (Galantucci et al., 2020; Inui and Tsubota, 2021). To emphasize the advantage of our GP-NS coupling to describe vortex interactions in superfluids without any phenomenological model, we also simulate the head-on collision of two superfluid vortex rings. In this case, superfluid vortex lines become distorted and their reconnection implies the exchange of parts of the lines and the formation of new tangled structures. This process is illustrated in Fig. 7. We use the same parameters as for the vortex ring case presented in Fig. 6 (c, d). Two vortex rings are seeded in the initial condition, with the same radius and opposite propagation directions. Vortex centers are shifted along the vertical axis, as in the recent simulation by Inui and Tsubota (2021), using LV-NS coupling methods. The mutual induction deforms the vortex rings when they approach to each other (Fig. 7a). The interaction (Fig. 7b) consists in the exchange of parts of each vortex line. After reconnection (Fig. 7c) the two new vortex rings are distorted and continue their movement following their original direction.

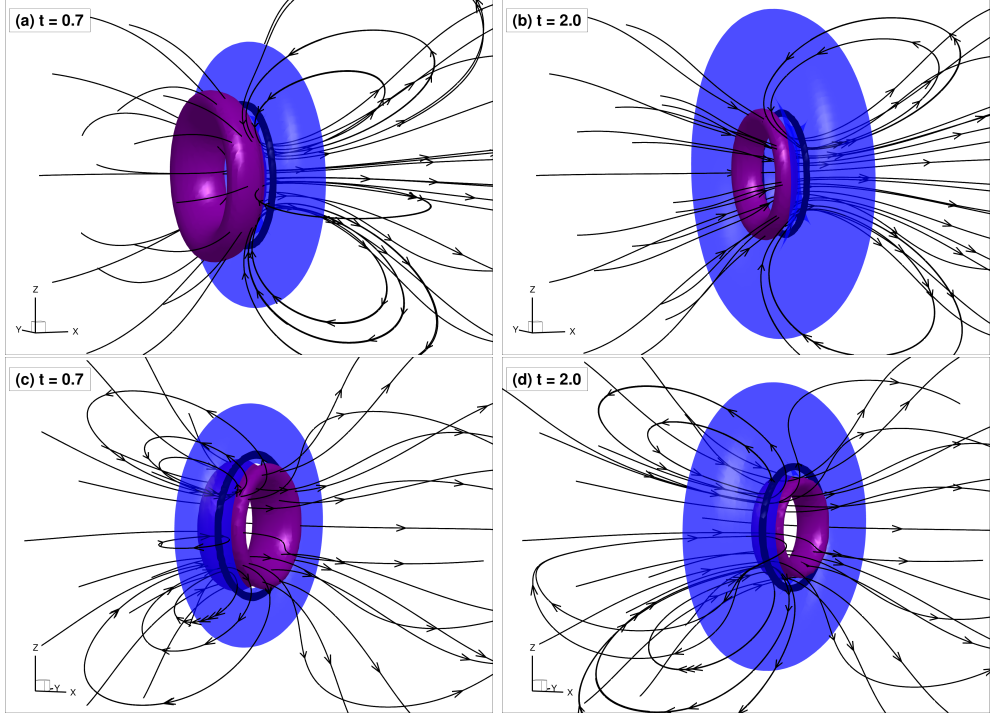


Figure 6: 3D evolution of a superfluid vortex ring in a normal fluid initially at rest. Snapshots for two time instants. Physical parameters  $\rho_n/\rho_s = 1$ ,  $B_{tab} = B'_{tab} = 0.4$ ,  $\eta_D = 0.035B_{tab}$  (panels a, b),  $B_{tab} = 0.4 > B'_{tab} = 0.1$ ,  $\eta_D = 0.05B_{tab}$  (panels c, d). Illustration of the triple-vortex structure. The superfluid vortex ring (in black) is identified by an iso-surface of low atomic density ( $0.5 |\psi|_{max}^2$ ). The two counter-rotating normal vortex rings are identified by iso-surfaces of normal fluid azimuthal vorticity: 0.03 for the blue outer ring and  $(-0.03)$  for the red inner ring. The streamlines in the normal fluid are also drawn. Mesh resolution  $128^3$ .

This complex interaction of superfluid vortex rings trigger in the normal fluid the formation of two pairs of normal vortex rings, that are attached to the quantized vortex ring and undergo the well-known *cut-and-connect* reconnection mechanism for viscous NS vortex tubes (Melander and Hussain, 1989; Hussain and Duraisamy, 2011). The obtained image of vortex interaction is qualitatively similar to that obtained by Inui and Tsubota (2021) using phenomenological models for vortex reconnection, but there are differences. In



particular, the repulsive motion observed when the two vortex ring are getting closer and before the connection is more intense than in LV-NS simulations. This affects the stretching of the normal fluid trapped between the two vortex rings. We recall that the superfluid vortex dynamics in our model obeys the GP equation, without any phenomenological assumption on the reconnection process.

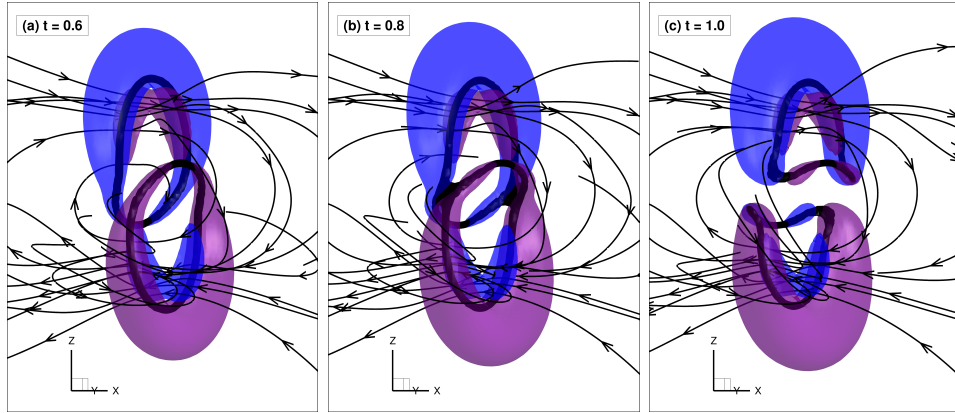


Figure 7: 3D head-on collision of two superfluid vortex ring in a normal fluid initially at rest. Snapshots for three time instants. Physical parameters  $\rho_n/\rho_s = 1$ ,  $B_{tab} = 0.4$ ,  $B'_{tab} = 0.1$ ,  $\eta_D = 0.05B_{tab}$ . Illustration of the structure of vortex reconnection. The superfluid vortex ring (in black) is identified by an iso-surface of low atomic density ( $0.2 |\psi|_{max}^2$ ). The two counter-rotating normal vortex rings are identified by iso-surfaces of normal fluid azimuthal vorticity:  $0.05$  for the blue outer ring and  $(-0.05)$  for the red inner ring. The streamlines in the normal fluid are also drawn. Mesh resolution  $128^3$ .

## 4 Conclusion

Recent models for the numerical simulation of two-fluid quantum flows (like helium II) were focused on coupling Navier-Stokes solvers for the normal fluid with vortex filaments methods for the superfluid fraction (Galantucci et al., 2020; Inui and Tsubota, 2021). These models consider that the superfluid dynamics is essentially described by line-vortex interactions (Biot-Savart law) and thus referred to as LV-NS models. The resulting main drawback is that vortex nucleation is absent from the description and superfluid vortex reconnections are necessarily based on phenomenological assumptions. We presented in this paper a model that links the Navier-Stokes (NS) normal flow dynamics to the Gross-Pitaevskii (GP) description of the superfluid fraction. The advantage of the model is that superfluid vortex dynamics is accurately and naturally described by the GP equation, as universally accepted in the literature. The new GP-NS coupling model is compatible with physical concepts (mutual friction force, source term in NS) used in LV-NS models, but redefined in the framework of the GP superfluid dynamics. The modified GP equation follows some ideas introduced by Coste (1998) to describe the compressible two-fluid liquid helium II, but it introduces new concepts: the regularized superfluid vorticity and velocity fields, the covariant gradient operator in the GP equation based on a slip velocity respecting the dynamics of vortex lines in the normal fluid.

The new GP-NS coupling model was implemented in a pseudo-spectral Fourier spectral code. Intensive tests validated the new numerical system against well-known benchmarks for the dynamics of different types or arrangements of quantized vortices (vortex crystal, vortex dipole and vortex rings) evolving in a normal fluid. The simulation of superfluid vortex head-on collision proved the ability of the method to account, without any phenomenological assumption, on the complex vortex interaction and reconnection. This new numerical model offers the possibility to revisit many fundamental phenomena established using the vortex filament method for superfluids (see the recent review by Tsubota et al. (2017)): reconnections of superfluid vortex lines in a NS fluid, movement of superfluid vortex bundles in a normal fluid, counter-flow quantum turbulence and, finally, two-fluid quantum turbulence.

## Acknowledgments

The authors acknowledge financial support from the French ANR grant ANR-18-CE46-0013 QUTE-HPC. Part of this work was performed using computing resources of CRIANN (Centre Régional Informatique et d'Applications Numériques de Normandie, France).

## References

## References

- L. Tisza, Transport phenomena in Helium II, *Nature* 141 (1938) 913.
- L. Landau, Theory of the superfluidity of Helium II, *Physical Review* 60 (1941) 356–358.
- C. Nore, M. Abid, M. E. Brachet, Decaying Kolmogorov turbulence in a model of superflow, *Physics of Fluids* 9 (1997a) 2644–2669.
- C. Nore, M. Abid, M. Brachet, Kolmogorov turbulence in low-temperature superflows, *Phys. Rev. Letters* 78 (1997b) 3896–3899.
- P. Clark di Leoni, P. D. Mininni, M. E. Brachet, Dual cascade and dissipation mechanisms in helical quantum turbulence, *Phys. Rev. A* 95 (2017) 053636.
- M. Kobayashi, P. Parnaudeau, F. Luddens, C. Lothodé, L. Danaila, M. Brachet, I. Danaila, Quantum turbulence simulations using the Gross-Pitaevskii equation: High-performance computing and new numerical benchmarks, *Computer Physics Communications* 258 (2021) 107579.
- N. G. Berloff, M. Brachet, N. P. Proukakis, Modeling quantum fluid dynamics at nonzero temperatures, *Proceedings of the National Academy of Sciences* 111 (2014) 4675–4682.
- I. Bekarevich, I. Khalatnikov, Phenomenological derivation of the equations of vortex motion in Helium II, *Sov. Phys. JETP* 13 (1961) 643.
- H. E. Hall, W. F. Vinen, D. Shoenberg, The rotation of liquid Helium II. I. Experiments on the propagation of second sound in uniformly rotating Helium

- II, Proceedings of the Royal Society of London. Series A. Mathematical and Physical Sciences 238 (1956a) 204–214.
- H. E. Hall, W. F. Vinen, D. Shoenberg, The rotation of liquid Helium II. II. The theory of mutual friction in uniformly rotating Helium II, Proceedings of the Royal Society of London. Series A. Mathematical and Physical Sciences 238 (1956b) 215–234.
- H. Adachi, S. Fujiyama, M. Tsubota, Steady-state counterflow quantum turbulence: Simulation of vortex filaments using the full Biot-Savart law, Phys. Rev. B 81 (2010) 104511.
- D. Kivotides, C. F. Barenghi, D. C. Samuels, Triple vortex ring structure in superfluid helium II, Science 290 (2000) 777–779.
- L. Galantucci, A. W. Baggaley, C. F. Barenghi, G. Krstulovic, A new self-consistent approach of quantum turbulence in superfluid helium, The European Physical Journal Plus 135 (2020) 547.
- J. Koplik, H. Levine, Vortex reconnection in superfluid helium, Phys. Rev. Lett. 71 (1993) 1375–1378.
- T. Frisch, Y. Pomeau, S. Rica, Transition to dissipation in a model of superflow, Phys.Rev.Lett. 69 (1992) 1644.
- S. Balibar, Laszlo Tisza and the two-fluid model of superfluidity, Comptes Rendus Physique 18 (2017) 586–591. Science in the making: The Comptes rendus de l’Académie des sciences throughout history.
- C. Coste, Nonlinear Schrödinger equation and superfluid hydrodynamics, The European Physical Journal B - Condensed Matter and Complex Systems 1 (1998) 245–253.
- E. B. Sonin, Magnus force in superfluids and superconductors, Phys. Rev. B 55 (1997) 485–501.
- C. Nore, M. Abid, M.-E. Brachet, Decaying Kolmogorov turbulence in a model of superflow, Phys. Fluids 9 (1997) 2644–2669.
- E. Sandier, S. Serfaty, Vortices in the Magnetic Ginzburg-Landau Model, BirkhÅduser Boston, 2007.

- W. Bao, Y. Cai, Mathematical theory and numerical methods for Bose-Einstein condensation, *Kinetic and related models* 6 (2013) 1–135.
- M. Tsubota, K. Fujimoto, S. Yui, Numerical studies of quantum turbulence, *J. of Low Temperature Physics* 188 (2017) 119–189.
- P. Parnaudeau, A. Suzuki, J.-M. Sac-Épée, GPS: An efficient & spectrally accurate code for computing Gross-Pitaevskii equation, *ISC-2015, Research Posters Session* (2015).
- D. Gottlieb, S. A. Orszag, *Numerical Analysis of Spectral Methods*, SIAM, Philadelphia, 1977.
- M. Frigo, S. Johnson, Design and implementation of FFTW3, *Proceedings of the IEEE* 93 (2005) 216–231.
- C. Nore, M. E. Brachet, E. Cerda, E. Tirapegui, Scattering of first sound by superfluid vortices, *Phys. Rev. Lett.* 72 (1994) 2593–2595.
- A. Griffin, V. Shukla, M.-E. Brachet, S. Nazarenko, Magnus-force model for active particles trapped on superfluid vortices, *Phys. Rev. A* 101 (2020) 053601.
- T. P. Billam, M. T. Reeves, B. P. Anderson, A. S. Bradley, Onsager-Kraichnan condensation in decaying two-dimensional quantum turbulence, *Phys. Rev. Lett.* 112 (2014) 145301.
- S. Inui, M. Tsubota, Coupled dynamics of quantized vortices and normal fluid in superfluid  $^4\text{He}$  based on the lattice Boltzmann method, *Phys. Rev. B* 104 (2021) 214503.
- M. V. Melander, F. Hussain, Cross-linking of two antiparallel vortex tubes, *Physics of Fluids A: Fluid Dynamics* 1 (1989) 633–636.
- F. Hussain, K. Duraisamy, Mechanics of viscous vortex reconnection, *Physics of Fluids* 23 (2011) 021701.
- C. F. Barenghi, R. J. Donnelly, W. F. Vinen, Friction on quantized vortices in Helium II. A review, *Journal of Low Temperature Physics* 52 (1983) 189–247.

## A Expression of the slip velocity

To solve Eq. (29), we use that  $\mathbf{v}_{\text{slip}}$  is perpendicular to the vortex line:  $\mathbf{v}_{\text{slip}} \cdot \boldsymbol{\Omega} = 0$ . We obtain:

$$-\rho_s \mathbf{v}_{\text{slip}} + \rho_n (B_\star (F\boldsymbol{\Omega} \times (\mathbf{w}_p - \mathbf{v}_{\text{slip}})) + B'_\star (\mathbf{w}_p - \mathbf{v}_{\text{slip}})) = 0, \quad (54)$$

or

$$-(\rho_s + B'_\star \rho_n) \mathbf{v}_{\text{slip}} - \rho_n B_\star F\boldsymbol{\Omega} \times \mathbf{v}_{\text{slip}} = -\rho_n (B_\star F\boldsymbol{\Omega} \times \mathbf{w} + B'_\star \mathbf{w}_p). \quad (55)$$

Setting

$$\mathbf{v}_{\text{slip}} = U_\star \mathbf{w}_p + V_\star F\boldsymbol{\Omega} \times \mathbf{w}, \quad (56)$$

we obtain that

$$\begin{aligned} & -(\rho_s + B'_\star \rho_n) (U_\star \mathbf{w}_p + V_\star F\boldsymbol{\Omega} \times \mathbf{w}) \\ & - \rho_n B_\star F\boldsymbol{\Omega} \times (U_\star \mathbf{w}_p + V_\star F\boldsymbol{\Omega} \times \mathbf{w}) \\ & = -\rho_n (B_\star F\boldsymbol{\Omega} \times \mathbf{w} + B'_\star \mathbf{w}_p) \end{aligned} \quad (57)$$

or, using that  $\boldsymbol{\Omega} \times (\boldsymbol{\Omega} \times \mathbf{w}) = \boldsymbol{\Omega} \times (\boldsymbol{\Omega} \times \mathbf{w}_p) = -\boldsymbol{\Omega} \cdot \boldsymbol{\Omega} \mathbf{w}_p$ ,

$$\begin{aligned} & -(\rho_s + B'_\star \rho_n) (U_\star \mathbf{w}_p + V_\star F\boldsymbol{\Omega} \times \mathbf{w}) \\ & - \rho_n B_\star F U_\star \boldsymbol{\Omega} \times \mathbf{w}_p + \rho_n B_\star F V_\star F\boldsymbol{\Omega} \cdot \boldsymbol{\Omega} \mathbf{w}_p \\ & = -\rho_n (B_\star F\boldsymbol{\Omega} \times \mathbf{w} + B'_\star \mathbf{w}_p). \end{aligned} \quad (58)$$

Taking the inner product with  $\mathbf{w}_p$  and  $\boldsymbol{\Omega} \times \mathbf{w}$ , we infer that

$$-(\rho_s + B'_\star \rho_n) U_\star + \rho_n B_\star V_\star F^2 \boldsymbol{\Omega} \cdot \boldsymbol{\Omega} = -\rho_n B'_\star, \quad (59)$$

$$-\rho_n B_\star U_\star - (\rho_s + B'_\star \rho_n) V_\star = -\rho_n B_\star. \quad (60)$$

The final solution is

$$U_\star = \frac{\rho_n (B_\star^2 F^2 \boldsymbol{\Omega} \cdot \boldsymbol{\Omega} \rho_n + B'_\star (\rho_s + \rho_n B'_\star))}{B_\star^2 F^2 \boldsymbol{\Omega} \cdot \boldsymbol{\Omega} \rho_n^2 + (\rho_s + \rho_n B'_\star)^2}, \quad (61)$$

$$V_\star = \frac{+B_\star \rho_n \rho_s}{B_\star^2 F^2 \boldsymbol{\Omega} \cdot \boldsymbol{\Omega} \rho_n^2 + (\rho_s + \rho_n B'_\star)^2}. \quad (62)$$

## B Expressions of friction coefficients

Friction coefficients  $U_\star$  and  $V_\star$  in Eq. (30) can be related to physical friction coefficients tabulated for superfluid helium II (Barenghi et al., 1983). We recall

that three different scales appear in our model: the healing length  $\xi$  that is also the scale of the vortex core, the smallest normal fluid length (the phonon/rotons mean free path)  $\lambda$  and the inter-vortex distance  $\ell$ . In LV-NS models, since a vortex is a filament,  $\xi = 0$  and  $\lambda < \ell$ . In HBVK models, the superfluid vorticity is averaged over a length scale larger than  $\ell$ . In our description, we average over some intermediate scale  $l$ , supposing that  $\xi < \lambda < l < \ell$ , to obtain a mesoscopic description of the mutual friction.

We consider the case of a uniform rotation and use the experimentally tabulated coefficients  $B_{tab}$  and  $B'_{tab}$  given by [Barenghi et al. \(1983\)](#). By averaging over the vortex array, we must identify:

$$B_{tab} = \frac{\rho}{\rho_n} V_\star, \quad (63)$$

$$B'_{tab} = \frac{\rho}{\rho_n} U_\star. \quad (64)$$

The above relations for  $(U_\star, V_\star)$  can be inverted into

$$B_\star = \frac{\rho_s V_\star}{\rho_n (\hat{\Omega}^2 V_\star^2 + (U_\star - 1)^2)}, \quad (65)$$

$$B'_\star = -\frac{\rho_s (\hat{\Omega}^2 V_\star^2 + (U_\star - 1)U_\star)}{\rho_n (\hat{\Omega}^2 V_\star^2 + (U_\star - 1)^2)}. \quad (66)$$

Using the that  $\hat{\Omega}^2 = 1$  on vortex lines, we finally find for our coefficients  $B_\star, B'_\star$ :

$$B_\star = \frac{\rho_s \frac{\rho_n}{\rho} B_{tab}}{\rho_n \left( \left( \frac{\rho_n}{\rho} B_{tab} \right)^2 + \left( \frac{\rho_n}{\rho} B'_{tab} - 1 \right)^2 \right)}, \quad (67)$$

$$B'_\star = -\frac{\rho_s \left( \left( \frac{\rho_n}{\rho} B_{tab} \right)^2 + \left( \frac{\rho_n}{\rho} B'_{tab} - 1 \right) \frac{\rho_n}{\rho} B'_{tab} \right)}{\rho_n \left( \left( \frac{\rho_n}{\rho} B_{tab} \right)^2 + \left( \frac{\rho_n}{\rho} B'_{tab} - 1 \right)^2 \right)}, \quad (68)$$

or

$$B_\star = \frac{B_{tab} \rho \rho_s}{\rho_n^2 (B_{tab}'^2 + B_{tab}^2) - 2B_{tab}' \rho \rho_n + \rho^2}, \quad (69)$$

$$B'_\star = \frac{B_{tab}' \rho \rho_s - \rho_n \rho_s (B_{tab}'^2 + B_{tab}^2)}{\rho_n^2 (B_{tab}'^2 + B_{tab}^2) - 2B_{tab}' \rho \rho_n + \rho^2}. \quad (70)$$

## C Movement of a 2D vortex dipole in a normal fluid

We consider the superfluid vortex dipole described in Sec. 3.1. In a periodic domain and in absence of normal fluid, the superfluid dipole moves in the  $x$ -direction with the velocity given by Eq. (51) (Griffin et al., 2020). Considering that the vortices of the dipole are straight lines perpendicular to the movement plane  $(x, y)$ , we can apply the force balance equation (20). We assume that the velocity induced by the vortex line is (in the vicinity of the line):

$$\mathbf{v}_s = u_s \mathbf{e}_x, \quad (71)$$

with  $u_s$  given by Eq. (51). Since the velocity of vortex lines is:

$$\mathbf{v}_L = \dot{x} \mathbf{e}_x + \dot{R} \mathbf{e}_y, \quad (72)$$

the tangent vector is  $s' = \mathbf{e}_z$  and the vorticity  $\mathbf{\Omega} = \omega_s \mathbf{e}_z$ , we can use Eqs. (19), (20), and (22) to obtain:

$$0 = \rho_s \omega_s \mathbf{e}_z \times (\mathbf{v}_L - \mathbf{v}_s) + \gamma_0 (\mathbf{v}_n - \mathbf{v}_L) + \gamma'_0 \mathbf{e}_z \times (\mathbf{v}_n - \mathbf{v}_L), \quad (73)$$

with  $\gamma_0 = \rho_n B_\star / F$  and  $\gamma'_0 = -\rho_n B'_\star$ . Assuming that  $\mathbf{v}_n = u_n \mathbf{e}_x$ , we separate from relation (73) the two linear equations corresponding to  $x$  and  $y$  directions, respectively:

$$0 = -\rho_s \dot{R} \omega_s + \gamma_0 (u_n - \dot{x}) + \dot{R} \gamma'_0, \quad (74)$$

$$0 = \rho_s \omega_s (\dot{x} - u_s) - \gamma_0 \dot{R} + \gamma'_0 (u_n - \dot{x}). \quad (75)$$

The solution is obtained in the form:

$$\dot{x}(t) = \frac{\gamma_0^2 \rho_s \omega_s (u_n - u_s)}{(\gamma_0^2 + (\gamma'_0 - \rho_s \omega_s)^2)(\rho_s \omega_s - \gamma'_0)} + \frac{u_s \rho_s \omega_s - \gamma'_0 u_n}{\rho_s \omega_s - \gamma'_0}, \quad (76)$$

$$\dot{R}(t) = \frac{\gamma_0 \rho_s \omega_s}{\gamma_0^2 + (\gamma'_0 - \rho_s \omega_s)^2} (u_n - u_s). \quad (77)$$

To follow the position  $x(t)$  and radius  $R(t)$  of the dipole in time, we calculate:

$$x(t) = \int_0^t \dot{x}(s) ds, \quad R(t) = \int_0^t \dot{R}(s) ds. \quad (78)$$